

## Attenuation of lightning-produced sferics in the Earth-ionosphere waveguide and low-latitude ionosphere

Brian S. Burkholder,<sup>1</sup> Michael L. Hutchins,<sup>1</sup> Michael P. McCarthy,<sup>1</sup> Robert F. Pfaff,<sup>2</sup> and Robert H. Holzworth<sup>1</sup>

Received 5 November 2012; revised 17 May 2013; accepted 20 May 2013; published 17 June 2013.

[1] We compare radio atmospherics (sferics) detected by the World Wide Lightning Location Network (WWLLN) to very low frequency (VLF) whistler waves observed in the low-latitude ionosphere by the Vector Electric Field Instrument of the Communications/Navigation Outage Forecasting System (C/NOFS) satellite. We also model the propagation of these sferics through the Earth-ionosphere waveguide to the subsatellite point using the Long-Wavelength Propagation Capability software and compare this result to the same C/NOFS data set. This unprecedentedly expansive data set allows comparison to theory and prior observation of VLF radio wave propagation in the Earth-ionosphere waveguide and low-latitude ionosphere. We show that WWLLN and C/NOFS observe the well-known effect of variable attenuation with direction within the Earth-ionosphere waveguide. Propagation within the ionosphere is also examined, and a lack of attenuation above 400 km is observed. Finally, in comparison to recent works using Detection of Electro-Magnetic Emissions Transmitted from Earthquake Regions (DEMETER) data by Fiser et al. and Chum et al., we find that C/NOFS successfully detects whistlers with comparable amplitudes at much greater distances, compared to those reported for DEMETER.

**Citation:** Burkholder, B. S., M. L. Hutchins, M. P. McCarthy, R. F. Pfaff, and R. H. Holzworth (2013), Attenuation of lightning-produced sferics in the Earth-ionosphere waveguide and low-latitude ionosphere, *J. Geophys. Res. Space Physics*, 118, 3692–3699, doi:10.1002/jgra.50351.

### 1. Introduction

[2] Lightning produces powerful, broadband radio waves called radio atmospherics, or just sferics, which propagate in the Earth-ionosphere waveguide and can be observed thousands of kilometers from the source. This makes sferics useful for obtaining the time, location, and energy of lightning strokes anywhere in the world, as is done by the World Wide Lightning Location Network (WWLLN) and other networks [Hutchins et al., 2012; Jacobson et al., 2006; Abarca et al., 2010]. In the ionosphere, these sferics couple to electron or ion whistler plasma waves below the respective cyclotron frequencies [Helliwell, 1965]. In the ionosphere, very low frequency (VLF) whistlers can propagate at all angles to the Earth's magnetic field (**B**), except within  $\sim 1^\circ$  of perpendicularity between the wave vector and **B**. These

waves are referred to as oblique whistlers when not aligned exactly with **B**.

[3] The wave dispersion is a function of the wave frequency, the ionosphere's electron density, the magnitude of the Earth's magnetic field, and the orientation of the whistler wave vector to the background field [Helliwell, 1965]. In situ study of these oblique whistler waves goes back decades, with observations of multipath whistlers [Gurnett et al., 1966] and interference bands from harmonics of the ion gyrofrequency [Shaw and Gurnett, 1971] by the INJUN satellite. Further study by the DE (Dynamics Explorer) satellite indicated a connection between lightning whistlers and ionospheric hiss [Sonwalkar and Inan, 1989]. The Wave Induced Particle Precipitation (WIPP) and Thunderstorm II and III rockets, with apogees up to  $\sim 400$  km, observed whistlers above the F peak but below the orbit of the Communications/Navigation Outage Forecasting System (C/NOFS) [Holzworth et al., 2011, 1999; Kelley et al., 1990, 1997]. Rocket payloads measured whistler dispersion [Holzworth et al., 1999] and the correlation with electron precipitation (via gyromagnetic resonance) [Arnoldy and Kintner, 1989]. Whistler waves have also been produced artificially by ground-based VLF transmitters like the one at Siple Station, Antarctica. These experiments also suggested a connection of whistler waves to magnetospheric hiss [Helliwell et al., 1986] and electron precipitation [Inan and Carpenter, 1987].

<sup>1</sup>Department of Earth and Space Sciences, University of Washington, Seattle, Washington, USA.

<sup>2</sup>Space Weather Laboratory, NASA Goddard Space Flight Center, Greenbelt, Maryland, USA.

Corresponding author: B. S. Burkholder, Department of Earth and Space Sciences, University of Washington, 4000 15th Ave. NE, Seattle, WA 98107, USA. (bburk2@uw.edu)

[4] More recently, the Detection of Electro-Magnetic Emissions Transmitted from Earthquake Regions (DEME-TER) satellite has been combined with the European Cooperation for Lightning Detection (EUCLID) lightning detection network to match whistlers measured in the ionosphere with strokes detected on the ground [Chum *et al.*, 2006]. This led to a study of whistler amplitude measured over thunderstorms, which found that amplitude was negatively correlated with distance from the stroke up to a range of  $\sim 500$  km and positively correlated with lightning current [Fiser *et al.*, 2010].

[5] We expand on previous rocket and satellite studies by using data from WWLLN and the C/NOFS satellite [Holzworth *et al.*, 2011; de La Beaujardire, 2004]. Work has already been done matching C/NOFS-detected whistlers with WWLLN-detected strokes and using WWLLN data to calculate stroke energy [Jacobson *et al.*, 2011a; Hutchins *et al.*, 2012]. The C/NOFS and WWLLN events can be correlated via a simple time-of-flight calculation, so that the stroke energy and whistler amplitude can be compared to theory with the assistance of the Long-Wavelength Propagation Capability (LWPC) software [Ferguson, 1998]. Theory and observation show that VLF waves propagating in the Earth-ionosphere waveguide attenuate as a function of distance and magnetic azimuth from the originating stroke, producing a marked amplitude difference between eastward propagation and westward propagation [Wait and Spies, 1960; Rybachek, 1995]. We are now able to detect this VLF propagation feature in lightning-generated sferics both within the Earth-ionosphere waveguide and in the topside ionosphere.

[6] By combining WWLLN's global lightning location data with the 12–24 s of burst waveform data C/NOFS regularly obtains during satellite eclipses, we achieve comprehensive observations of whistlers and sferics. By comparing stroke energy with whistler amplitude, we will show that the sferic waves traveling to the east in the Earth-ionosphere waveguide experience less attenuation than those traveling to the west and are more likely to be observed at all but the shortest distances to the originating stroke, while westward going waves introduce comparatively more energy to the topside ionosphere, as predicted by theory but never adequately measured [Wait and Spies, 1960; Rybachek, 1995]. Additionally, we will show that attenuation in the ionosphere is dominated by the D and E regions, below the orbit of C/NOFS, with little further attenuation between 400 and 850 km.

## 2. Instruments and Methods

### 2.1. The World Wide Lightning Location Network

[7] WWLLN (see <http://wwlln.net> for more information) consists of more than 60 VLF radio receivers spread around the world. It uses the time-of-group-arrival technique to time and locate strokes. The network is capable of seeing both in-cloud and cloud-to-ground (CG) strokes, achieving 30–50% detection efficiency for strokes above 40 kA (it observes 10–15% of all global cloud-to-ground strokes) [Hutchins *et al.*, 2012]. Stroke times and locations are accurate within 5 km and 10  $\mu$ s [Hutchins *et al.*, 2012]. Source stroke radiated VLF energy of WWLLN-located strokes is also determined and is used to estimate a mean VLF power

in the 1.33 ms window over which energy is integrated [Hutchins *et al.*, 2012].

### 2.2. The Vector Electric Field Instrument

[8] The Vector Electric Field Instrument (VEFI) on C/NOFS consists of three orthogonal pairs of boom antennas: two in the orbital plane at  $45^\circ$  to nadir and the last perpendicular to the orbital plane [de La Beaujardire, 2004]. The instrument measures broadband VLF waves at frequencies up to 16 kHz in short burst samples every orbit. Such data are collected only when the satellite is in eclipse. This is referred to as the burst mode, which records data up to 32 kilosamples per second for 12–24 s intervals. About 30,000 whistlers are included in this study, drawn from 20% of all C/NOFS bursts.

### 2.3. Whistler-Stroke Correlation

[9] Lightning sferics initially propagate either outward horizontally from their source within the Earth-ionosphere waveguide or directly vertically. As a sferic in the Earth-ionosphere waveguide couples to an ionospheric whistler mode, the wave vector rotates into the vertical by Snell's law and is within  $10^\circ$  of zenith at the time it reaches the satellite altitude, per the index of refraction supplied by Helliwell [1965, p. 29]. Thus, although C/NOFS's orbital inclination is  $13.5^\circ$  (i.e., nearly equatorial), the sferic waves it observes can originate from nearly any part of the globe (though strokes closer to the subsatellite track are more easily observed). This analysis is valid only in the far field, requiring that the wavelength be less than the distance between the surface of the Earth and the ionosphere. The lowest frequency in this study is 6 kHz, corresponding to a wavelength of 50 km, so the far-field condition is met. Note that while, in reality, the ray path may diverge from the direction of the wave vector [Maeda and Kimura, 1959], we take as an approximation that all the ionospheric whistler propagation is purely vertical.

[10] C/NOFS directly measures the whistler waveform using VEFI and the lightning source time using the optical lightning detector for lightning events within the optical field of view [Jacobson *et al.*, 2011b] but does not determine the accurate source stroke location. We have correlated the VEFI whistlers with WWLLN lightning source strokes in order to trace the whistlers' paths through the Earth-ionosphere waveguide and the ionosphere. This is done via a simple time-of-flight calculation. It can be assumed, to first order, that the sferic travels in the Earth-ionosphere waveguide from the stroke location to the subsatellite point along a great circle path, where the upward coupled wave's wave vector turns into a vertical according to Snell's law. This method ignores the group path in favor of the (simpler) wave vector. Though this does not reveal the precise path taken by whistlers through the ionosphere, it is sufficient to match C/NOFS and WWLLN events, as detailed by Jacobson *et al.* [2011a]. The wave travels the subionospheric path at nearly the speed of light. The ionosphere, however, imposes a much slower group speed for the coupled whistler wave than that in the Earth-ionosphere waveguide. The ionospheric delay is obtained by looking at the dispersion of whistlers measured at the satellite. Because the group delay of a wave with frequency  $f$  is proportional to  $1/\sqrt{f}$ , the time at which the vertically propagating whistler would have arrived at the

satellite if it were unaffected by the ionospheric plasma can be estimated (i.e., the time of flight at the vacuum speed of light) [Helliwell, 1965, p. 32]. This enables comparison to the time-of-flight calculation, counting as a match any whistler whose detected time at C/NOFS (adjusted by the delay proportional to  $1/\sqrt{f}$  and subionospheric travel time) is between 0 and 3 ms later than the time of the WWLLN stroke. This matching method was described and validated by Jacobson *et al.* [2011a].

[11] The data set discussed in this paper contains data from July 2009 to September 2011. The C/NOFS data are processed automatically via the automatic whistler detection program described by Jacobson *et al.* [2011a]. From C/NOFS, we are able to calculate the average energy (proportional to the time-integrated square of the electric field amplitude) of each whistler, while we obtain the lightning stroke radiated VLF energy from the method of Hutchins *et al.* [2012]. Sferic root-mean-square (RMS) amplitude at the subsatellite point is then obtained from the WWLLN lightning source power data using the U.S. Navy VLF propagation code LWPC (Long-Wavelength Propagation Capability) [Ferguson, 1998]. In order to compare the C/NOFS and WWLLN data, the WWLLN VLF energy measured in a 1.33 ms window was propagated to the C/NOFS subsatellite point. This was done using the LWPC code, as used for the WWLLN stroke energy calculations [see Hutchins *et al.*, 2012]. Because LWPC requires a monochromatic source, the resulting electric field at the subsatellite point (using the location of C/NOFS at the time the satellite detected the stroke in question) was calculated for frequencies between 6 and 16 kHz, in 1 kHz intervals. The mean square amplitude ( $E^2$ ) for these 11 frequencies was calculated and is the value reported as the square of the subsatellite amplitude. Then the Poynting flux,

$$S = \frac{1}{2} \frac{n}{Z_0} E^2, \quad (1)$$

is calculated at both C/NOFS and the subsatellite point, where  $Z_0 = 377 \Omega$  is the vacuum impedance and  $n$  is the index of refraction equal to unity at the subsatellite point and given by

$$n = \sqrt{\left(1 + \frac{\omega_{pe}^2}{\omega(\omega_{ce} \cos \theta - \omega)}\right)}, \quad (2)$$

at C/NOFS [Helliwell, 1965]. In equation (2),  $\omega_{pe}$  is the electron plasma frequency,  $\omega_{ce}$  is the electron cyclotron frequency,  $\omega$  is the angular wave frequency (taken to be  $2\pi \cdot 10^4$  rad/s), and  $\theta$  is the angle between the Earth's magnetic field  $\mathbf{B}$  and the wave vector  $\mathbf{k}$  (where, again,  $\mathbf{k}$  is taken to be purely vertical as a simplifying assumption). The Earth's magnetic field (needed for  $\omega_{ce}$  and  $\cos \theta$ ) is obtained from the International Geomagnetic Reference Field model, while the electron density (needed for  $\omega_{pe}$ ) is obtained from the Coupled Ion-Neutral Dynamics Investigation instruments on C/NOFS [Klenzing *et al.*, 2011].

### 3. Discussion

[12] The theory of propagation within the Earth-ionosphere waveguide is well known [Wait and Spies, 1960; Rybachek, 1995]. What is unprecedented is the combination of global lightning data with the frequent VLF burst

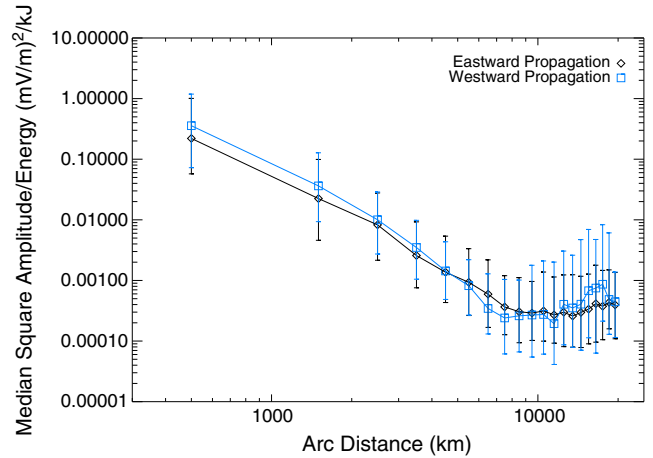


**Figure 1.** Median ratio within each bin of whistler square amplitude measured at C/NOFS to energy of the associated WWLLN stroke, in 1000 km bins. Both eastward and westward propagating waves' amplitudes decline at the same rate up to  $\sim 10,000$  km and then rise again. Bars represent first and third quartiles.

measurements of C/NOFS. This enables data collection from strokes in all areas of the world, as well as all times of day and various geomagnetic conditions. This insures that our data are free of any potential geographic or temporal biases.

#### 3.1. Variation of Sferic and Whistler Properties With Stroke Power and Distance

[13] Figure 1 shows the median ratio within each 1000 km bin of whistler mean amplitude squared (proportional to energy) at C/NOFS to WWLLN stroke energy. This ratio decreases as a function of arc distance between the stroke and subsatellite point up to one quarter of the way around the world ( $\sim 10,000$  km). At greater distances, the ratio begins to increase as the waves reconverge, as shown by Jacobson *et al.* [2011a]. Figure 2 shows the whistler electric field amplitude squared at C/NOFS as a function of WWLLN source stroke energy. Greater stroke energy corresponds to greater whistler amplitude, as expected. The events are also binned by arc distance (up to 5000 km), showing that a given stroke energy produces stronger whistlers the closer the stroke is to the subsatellite point (for these distances). We see that the observed amplitude of the topside whistler waves increases with the energy of the associated WWLLN stroke as expected and is in agreement with the results of Fiser *et al.* [2010].

#### 3.2. Variation of Sferic and Whistler Properties With Direction of Propagation

[14] The ionosphere affects propagation within the Earth-ionosphere waveguide, introducing a directional bias in the amplitude of propagating sferics. Specifically (in the frequency range measured by C/NOFS,  $< 16$  kHz), waves propagating from the geographic west to the geographic east (that is, eastward propagating) experience the least attenuation, while those traveling from east to west (westward propagating) experience the most attenuation, with continuous variation between these two antiparallel extremes [Wait and Spies, 1960]. Wait and Spies [1960] attribute this effect

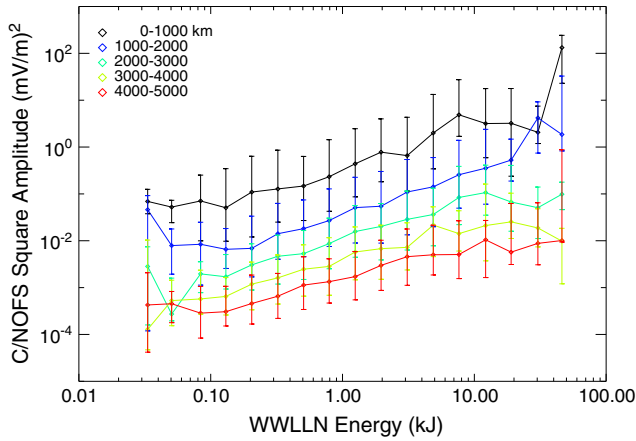


**Figure 2.** Median whistler square amplitude at C/NOFS as a function of WWLLN stroke energy. Whistler amplitude in the ionosphere increases as a function of WWLLN energy and is higher for strokes closer to the subsatellite point. Bars are first and third quartiles. Bins are evenly spaced in the log space, with the energy increasing by 0.2 with each bin.

to the direction of the sferic with respect to the Earth's magnetic field.

[15] This effect is observable in the combined C/NOFS-WWLLN data set. We calculate the heading from every stroke to its respective subsatellite point and keep those events whose heading (reckoned at the stroke location) is within  $45^\circ$  of due east or due west (henceforth referred to as eastward and westward propagating waves, respectively). The majority of data (78%) is retained, because of the location of C/NOFS and the distribution of global lightning. C/NOFS's orbital inclination is  $13^\circ$ , and the bulk of global lightning is produced at low latitudes [Boccippio *et al.*, 2000]. Thus, most detected sferics travel considerably farther in the east/west direction than in the north/south and are included in our direction selection.

[16] The east-west difference is apparent in Figure 3, which shows a histogram of the C/NOFS-WWLLN data set in 200 km bins by arc distance between the source stroke and subsatellite point. We see that westward propagating sferics are slightly more prevalent than eastward propagating ones within the first 2000 km from the source. In Figure 3, we see that the number of westward propagating waves (the blue, dashed line in Figure 3) peaks near 3000 km, which is well before the peak of the eastward propagating waves (the red, solid line in Figure 3). Note that because lightning is more prevalent at dusk than at dawn and because C/NOFS records data only during satellite eclipses, there is an inherent anisotropy in the location of global lightning relative to C/NOFS [Lay *et al.*, 2007]. More eastward propagating sferics (coming from the duskside) are created than westward propagating ones (coming from the dawnside). In order to disentangle the effect of lightning distribution from that of propagation, we have found that for all lightning strokes occurring within 100 ms of a C/NOFS VLF event (regardless of whether any given stroke actually maps to said event), 55% occur west of the subsatellite point, while only 45% occur to the east. This disparity arises solely from the global distribution of lightning relative to C/NOFS.

We take this as a control population and thus multiply the histograms of eastward and westward propagating sferics by 10/11 and 10/9, respectively. This serves to eliminate any anisotropic effect due to the location of lightning, leaving only effects due to propagation in the Earth-ionosphere waveguide. These are the data shown in Figure 3. This correction makes only a small difference, and there is substantial difference remaining between the two populations. To test the significance of this difference, we use a chi-square test, first scaling the westward distribution to have the same total number of events as the eastward distribution. The null hypothesis that the two data sets are derived from the same distribution can be rejected with probability greater than 0.999. This remains true if we restrict the analysis to, e.g., a 4000 km range from the source (using only that range to normalize the distributions). After peaking, the number of observed westward traveling sferics falls off rapidly compared to eastward traveling ones, leaving eastward traveling sferics consistently more likely to be detected at larger distances. We speculate that this may be because at short distances ( $<2000$  km), sferics have experienced relatively little attenuation and thus the likelihood of detecting a simultaneous C/NOFS-WWLLN event is dominated by the amount of energy put into the ionosphere. This is greater for westward propagating waves. This may be because these waves better couple into the whistler mode, and so they are more readily observed by C/NOFS at short distances. At larger distances, the greater incidence of eastward propagating whistlers may be because eastward propagating sferics experience less Earth-ionosphere waveguide attenuation than westward propagating ones and are thereby more intense and easier to detect. This is all consistent with the observation of Jacobson *et al.* [2008] that ionospheric reflectivity has a

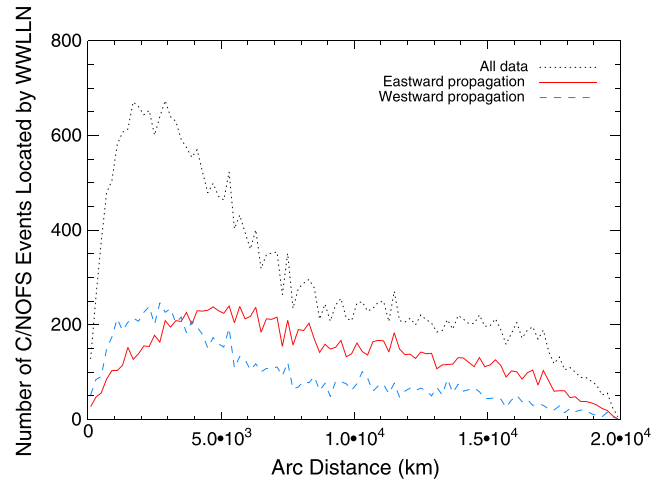


**Figure 3.** Histogram of all whistlers observed at C/NOFS with associated WWLLN events, binned according to the arc distance between the stroke and the subsatellite point. We see that the number of counts peaks quickly and then falls before leveling off from about 8000 to 20,000 km. Using sferic waves propagating within  $45^\circ$  of eastward or westward shows the westward propagating waves peaking closer to the source than the eastward propagating waves before falling off more quickly. Data have been corrected to reflect the anisotropic distribution of global lightning.

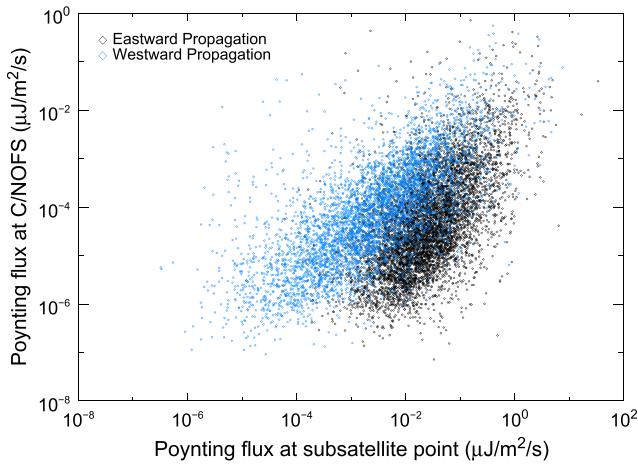


**Figure 4.** Scatterplot of Poynting flux of C/NOFS whistlers versus Poynting flux of sferics at the subsatellite point as calculated by LWPC. This shows a substantial energy loss between the subsatellite point and the satellite, which we attribute to coupling between the Earth-ionosphere waveguide and the ionosphere. Note that for this plot, data are restricted to those strokes which occurred between 1000 and 8000 km from the subsatellite point, the range in which LWPC produces high-quality results.

maximum for eastward propagating waves and a minimum for westward propagating ones.

[17] If the LWPC prediction of the Earth-ionosphere waveguide propagation is correct, then Figure 4 gives clear observational evidence that westward propagating sferics couple more strongly into transionospheric whistlers. On the other hand, if the waveguide propagation is not correctly modeled, then this conclusion is not necessarily true. However, WWLLN data suggest that this effect is physical. In addition to the data shown in Figure 3, data from the WWLLN stations in Hawaii and Fiji (so that the propagation path to the station is isotropic) were examined and show that eastward propagating sferics are more numerous, more energetic, and observed at greater distances. Thus, we feel confident accepting the predictions of LWPC. Note also that Figure 4 contains only strokes between 1000 and 8000 km away from the subsatellite point. This is because LWPC produces its best results in this range, as discussed by *Hutchins et al.* [2012]. The lower bound is necessary in order to make sure that the waves are well into the far field and hence have coupled into the Earth-ionosphere waveguide. Note that this is a very conservative limit. The upper bound is because LWPC was validated by examining transmission over the Pacific, at a range of  $\sim 8000$  km [Ferguson, 1995]. Thus, LWPC calculations at larger distances have not been experimentally verified.

[18] We see in Figure 5 a histogram of all data in this study, binned according to the ratio of whistler amplitude squared to the associated stroke's energy. Eastward propagating waves have a ratio that peaks approximately 1 order of magnitude lower than that of westward propagating waves. That is, for a fixed WWLLN stroke energy, a whistler produced by an eastward propagating sferic will be weaker than a whistler produced by a westward propagating sferic (though the whistlers from eastward propagating

sferics are more numerous). This is consistent with attenuation within the Earth-ionosphere waveguide being due to coupling to ionospheric wave modes. Only a portion of a sferic is transmitted through the bottom of the ionosphere (and therefore lost to further subionospheric propagation). The reflected portion continues on in the Earth-ionosphere waveguide, with the rest being transmitted into the ionosphere. An anisotropic reflection coefficient, like that found by *Jacobson et al.* [2008], can thus explain why whistlers from eastward propagating waves are weaker yet more readily detected. More energy enters the ionosphere for westward propagating sferics than for eastward propagating ones. Whistler amplitude at C/NOFS will then be proportional to the attenuation experienced by the sferic (i.e., the transmission coefficient for the particular wave path), as energy lost from the waveguide shows up in the ionosphere. Therefore, the likelihood of observing a combined C/NOFS-WWLLN event is driven by the wave amplitude in the Earth-ionosphere waveguide at the subsatellite point, and so eastward propagating waves are the most readily observed at all but the shortest distances. One potentially confounding factor is energy loss due to collisions within the ionosphere. These will be mostly electron-neutral collisions below  $\sim 150$  km altitude and mostly electron-ion collisions above [Aggarwal et al., 1979]. This effect may be anisotropic but cannot be examined by this study.

[19] Back in Figure 1, we compared the ratios of C/NOFS amplitude to WWLLN energy for eastward and westward propagating waves as a function of arc distance from the source. The difference between eastward and westward propagating waves is well within a quartile of the median for every arc distance bin. This similarity is something of a surprise given the clear attenuation disparity shown in Figure 3. We do, however, observe the amplitude minimum a quarter of the way around the world from the source and the subsequent secondary maximum at  $\sim 20,000$  km.

[20] This long-distance detection stands in contrast to that in *Fiser et al.* [2010], using the DEMETER satellite. They were unable to observe whistlers at distances greater

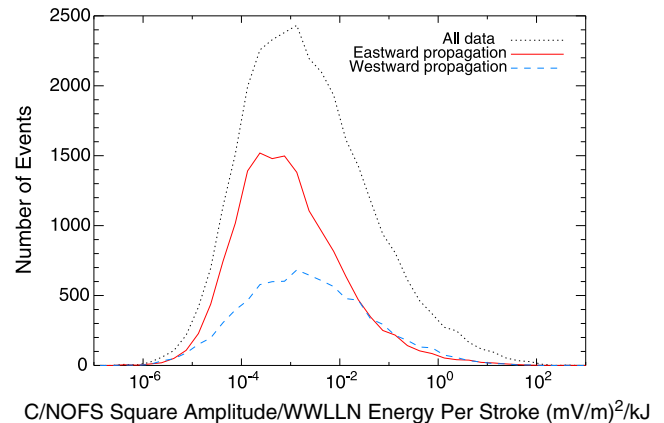


**Figure 5.** Histogram of the ratio of whistler square amplitude measured at C/NOFS to energy of the associated WWLLN stroke. There are about 30% fewer westward propagating strokes than eastward propagating ones. Additionally, the center of the westward peak is a factor of 5 higher than that of the eastward peak.

than  $\sim 1000$  km between the source stroke and subsatellite point. Whistlers observed by C/NOFS do not attain minimum amplitude until a distance of  $\sim 10,000$  km from the source, and then they intensify at greater distances. Despite the different range of arc distances over which whistlers are detected, Figure 2 shows that there is agreement between the whistler amplitudes measured by C/NOFS and WWLLN. We show a linear relationship between stroke energy and C/NOFS square amplitude. But, the relationship between stroke power (for this purpose taken to be the stroke energy divided by a 1.33 ms time window) and stroke current has been shown to have the empirical form

$$P_{\text{stroke}} = 1.676 \times |I_{\text{peak}}|^{1.62}, \quad (3)$$

for WWLLN, where  $P_{\text{stroke}}$  has units of kilowatts and  $I_{\text{peak}}$  has units of kiloamperes [Hutchins *et al.*, 2012]. We thus find, similar to Fiser *et al.*, that whistler amplitude increases nonlinearly with stroke current. The whistler amplitudes observed by C/NOFS are comparable to those observed by DEMETER. At a distance of  $\sim 200$  km between the source stroke and DEMETER's subsatellite point, whistlers with amplitudes between 0.1 and 0.3 mV/m were observed for stroke current up to 30 kA. For comparable strokes (radiated VLF power up to  $\sim 400$  kW corresponding to 0.4 kJ), C/NOFS observes root median square whistler amplitudes between  $\sim 0.1$  and  $\sim 0.3$  mV/m.

### 3.3. Variation of Whistler Amplitude With Altitude

[21] C/NOFS's variable altitude within the ionosphere makes it possible to observe changes in whistler attenuation as a function of altitude. Whistler attenuation in the ionosphere occurs when charged particles accelerated by the wave collide with neutrals, transferring energy out of the whistler mode. Additionally, energy can be transferred in three-wave processes, in which the upgoing whistler decays into other wave modes. The bulk of these colli-

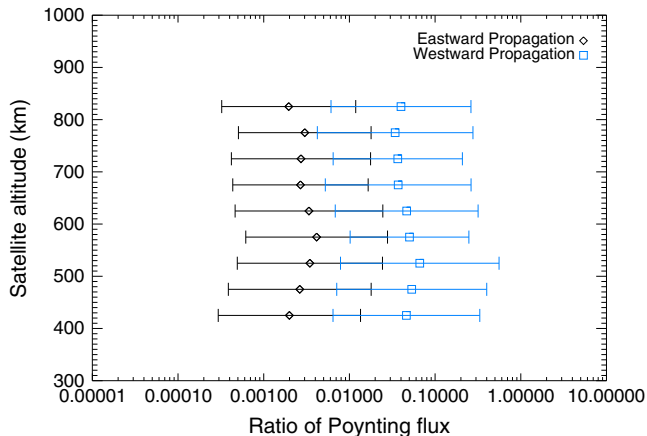


**Figure 6.** Mean whistler Poynting flux at C/NOFS divided by LWPC Poynting flux at the subsatellite point in 50 km altitude bins, with bars at one standard deviation. Considerable east/west variation is apparent. There is no variation with altitude, indicating that no meaningful attenuation occurs between 400 and 850 km. Only events with stroke to subsatellite arc distance between 1000 and 8000 km are used here, as that is the regime in which LWPC is most effective.

**Table 1.** Fit Parameters for Equation (4)<sup>a</sup>

	$a$	$b$
East	$-2.99 \pm 0.02$	$0.83 \pm 0.01$
West	$-2.30 \pm 0.03$	$0.69 \pm 0.01$

<sup>a</sup>Fit parameters for equation (4) showing the difference in Poynting flux between ground and satellite, for both eastward propagation and westward propagation. This is the result of both reflection at the bottom of the ionosphere and attenuation within the ionosphere. The given error is the  $1 \sigma$  uncertainty. This includes only data between 1000 and 8000 km, where LWPC produces its highest-quality results.

sions or three-wave processes appear to occur below 400 km [Helliwell, 1965; Thrane and Piggott, 1966]. Figure 6 shows that whistler energy remains effectively constant across the 400 to 850 km altitude range of the satellite. This indicates that the effect of ionospheric plasma between 400 and 850 km has a negligible contribution to overall whistler attenuation, a result which is unsurprising but has not been adequately measured previously. Additionally, Figures 4 and 6 show that whistlers from westward propagating sferics are consistently more energetic than whistlers from eastward propagating sferics for a given input energy. This result is consistent with the differences between eastward propagation and westward propagation discussed above. As Figure 6 shows, the separation in means is greater than the size of one standard deviation in each bin, with overall ratios of  $10^{-2.5 \pm 0.9}$  for eastward propagating waves and  $10^{-1.3 \pm 0.8}$  for westward propagating waves. Though these ranges do overlap, the mean for eastward propagation is outside the error bounds for westward propagation and vice versa. This demonstrates that for a given input energy, whistler waves coupled from westward propagating sferics are stronger than those coupled from eastward propagating sferics. Since westward propagating sferics are, on the whole, weaker than eastward propagating ones, this demonstrates the possibility that attenuation in the Earth-ionosphere waveguide is partially the result of energy loss to the ionosphere.

[22] Additionally, we see in Figure 4 that the amplitude at the satellite is reduced considerably from the amplitude at the subsatellite point, as a result of both the small amount of energy transmitted through the bottom of the ionosphere and energy loss in the ionosphere. Note that the results displayed in Figure 4 are approximate, as we have assumed that the wave path is purely vertical. In reality, the whistler group path diverges from the vertical, and so the subsatellite point is not where transmission to the ionosphere occurs [Santolik *et al.*, 2009]. However, since the horizontal distance traversed in the ionosphere by a whistler can be as low as the order of 100 km [Santolik *et al.*, 2009], the following comparison can still give a useful approximation of the fraction of wave energy introduced to the ionosphere via whistler waves. A ray tracing model in the ionosphere would be necessary to precisely match whistlers to their entry points into the ionosphere. The relationship between Poynting fluxes at C/NOFS and at the subsatellite point is given empirically by

$$S_{\text{C/NOFS}} = 10^a \cdot (S_{\text{LWPC}})^b, \quad (4)$$

where  $S_{\text{C/NOFS}}$  is the whistler Poynting flux measured by C/NOFS and  $S_{\text{LWPC}}$  is the sferic Poynting flux calculated at the subsatellite point by LWPC from WWLLN source

energy. Both are in units of  $\mu\text{J}/\text{m}^2/\text{s}$ . This fit is linear on a log-log scale. Values for the parameters  $a$  and  $b$  are given in Table 1. We see that a whistler wave at the satellite with a Poynting flux of, e.g.,  $10^{-4} \mu\text{J} \cdot \text{m}^{-2} \cdot \text{s}^{-1}$  corresponds to a subsatellite Poynting flux of  $\sim 6 \times 10^{-2} \mu\text{J} \cdot \text{m}^{-2} \cdot \text{s}^{-1}$  for eastward propagating sferics but only  $\sim 4 \times 10^{-3} \mu\text{J} \cdot \text{m}^{-2} \cdot \text{s}^{-1}$  for westward propagating ones. By comparison, producing a whistler with a Poynting flux of  $10^{-1} \mu\text{J} \cdot \text{m}^{-2} \cdot \text{s}^{-1}$  at the satellite requires an eastward propagating sferic with  $\sim 3 \times 10^2 \mu\text{J} \cdot \text{m}^{-2} \cdot \text{s}^{-1}$  or a westward propagating sferic with only  $\sim 8 \times 10^1 \mu\text{J} \cdot \text{m}^{-2} \cdot \text{s}^{-1}$ . Note that if this empirical fit continues to be valid at high values of subsatellite Poynting flux, then these two curves will intersect at a subsatellite Poynting flux of about  $9.7 \times 10^4 \mu\text{J} \cdot \text{m}^{-2} \cdot \text{s}^{-1}$ . Above this value, the relationship between the whistlers coupled from eastward and westward traveling sferics would switch, with eastward propagating sferics producing more intense whistlers for a given input energy.

#### 4. Conclusions

[23] The combination of WWLLN-located strokes with C/NOFS-detected whistlers provides the ability to examine the effects of the ionosphere and Earth-ionosphere waveguide on the propagation of VLF waves. Within the Earth-ionosphere waveguide, we have shown the effects of sferic heading and distance between the stroke and subsatellite point on wave amplitude. This demonstrates that some of the energy lost by sferics within the Earth-ionosphere waveguide is gained by whistlers in the ionosphere, so that sferics that experience more attenuation correspond to more energetic whistlers. Within the ionosphere, we have shown an approximately 3 order of magnitude loss of energy from the subsatellite point to C/NOFS but a lack of attenuation caused by the ionosphere between 400 and 850 km. This matches prior observation.

[24] We have additionally made comparison to the work of Fiser et al. with DEMETER. We find qualitative agreement with their observation of the nonlinear dependence of whistler amplitude on stroke current. However, where DEMETER observed whistlers disappearing into the noise at distances greater than  $\sim 1000$  km, C/NOFS observes minimum whistler amplitude at  $\sim 10,000$  km and continues observing whistlers all the way up to  $\sim 20,000$  km.

[25] **Acknowledgments.** The authors wish to thank the World Wide Lightning Location Network (<http://wwlln.net>), a collaboration among over 50 universities and institutions, for providing the lightning location data used in this paper. This research was supported in part by AFOSR grant FA955009-1-0309, NASA grant NNX08AD12G, and DARPA grant HR0011-10-1-0060.

[26] Robert Lysak thanks Carl Siefring and another reviewer for their assistance in evaluating this paper.

#### References

Abarca, S. F., K. L. Corbosiero, J. Galarneau, and J. Thomas (2010), An evaluation of the Worldwide Lightning Location Network (WWLLN) using the National Lightning Detection Network (NLDN) as ground truth, *J. Geophys. Res.*, *115*, D18206, doi:10.1029/2009JD013411.

Aggarwal, K., N. Nath, and C. Setty (1979), Collision frequency and transport properties of electrons in the ionosphere, *Planet. Space Sci.*, *27*(6), 753–768.

Arnoldy, R. L., and P. M. Kintner (1989), Rocket observations of the precipitation of electrons by ground VLF transmitters, *J. Geophys. Res.*, *94*(A6), 6825–6832, doi:10.1029/JA094iA06p06825.

Boccippio, D. J., S. J. Goodman, and S. Heckman (2000), Regional differences in tropical lightning distributions, *J. Appl.*, *39*(12), 2231–2248, doi:10.1175/1520-0450(2001)040<2231:RDITLD>2.0.CO;2.

Chum, J., F. Jiricek, O. Santolik, M. Parrot, G. Diendorfer, and J. Fiser (2006), Assigning the causative lightning to the whistlers observed on satellites, *Ann. Geophys.*, *24*(11), 2921–2929.

de La Beaujardiere, O. (2004), C/NOFS: A mission to forecast scintillations, *J. Atmos. Sol. Terr. Phys.*, *66*(17), 1573–1591, doi:10.1016/j.jastp.2004.07.030.

Ferguson, J., (1998), Computer programs for assesment of long-wavelength radio communications, version 2.0, *Technical report*, Space and Nav. Warfare Syst. Cent. Center, San Diego, Calif.

Ferguson, J. A. (1995), Ionospheric model validation at VLF and LF, *Radio Sci.*, *30*(3), 775–782, doi:10.1029/94RS03190.

Fiser, J., J. Chum, G. Diendorfer, M. Parrot, and O. Santolik (2010), Whistler intensities above thunderstorms, *Ann. Geophys.*, *28*(1), 37–46.

Gurnett, D. A., S. D. Shawhan, and G. W. Pfeiffer (1966), Hook whistler—A new equatorial whistler observed by Injun 3, *Nature*, *212*(5069), 1442–1443, doi:10.1038/2121442a0.

Helliwell, R. A. (1965), *Whistlers and Related Ionospheric Phenomena*, Stanford Univ. Press, Stanford, Calif.

Helliwell, R. A., D. L. Carpenter, U. S. Inan, and J. P. Katsufakis (1986), Generation of band-limited VLF noise using the Siple transmitter—A model for magnetospheric hiss, *J. Geophys. Res.*, *91*(A4), 4381–4392, doi:10.1029/JA091iA04p04381.

Holzworth, R. H., R. M. Winglee, B. H. Barnum, Y. Q. Li, and M. C. Kelley (1999), Lightning whistler waves in the high-latitude magnetosphere, *J. Geophys. Res.*, *104*(A8), 17,369–17,378, doi:10.1029/1999JA900160.

Holzworth, R. H., M. P. McCarthy, R. F. Pfaff, A. R. Jacobson, W. L. Willcockson, and D. E. Rowland (2011), Lightning-generated whistler waves observed by probes on the Communication/Navigation Outage Forecast System satellite at low latitudes, *J. Geophys. Res.*, *116*, A06306, doi:10.1029/2010JA016198.

Hutchins, M. L., R. H. Holzworth, C. J. Rodger, and J. B. Brundell (2012), Far-field power of lightning strokes as measured by the World Wide Lightning Location Network, *J. Atmos. Oceanic Technol.*, *29*(8), 1102–1110, doi:10.1175/JTECH-D-11-00174.1.

Inan, U. S., and D. L. Carpenter (1987), Lightning-induced electron-precipitation events observed at l-approximately-2.4 as phase and amplitude perturbations on subionospheric VLF signals, *J. Geophys. Res.*, *92*(A4), 3293–3303, doi:10.1029/JA092iA04p03293.

Jacobson, A. R., R. Holzworth, J. Harlin, R. Dowden, and E. Lay (2006), Performance assessment of the World Wide Lightning Location Network (WWLLN), using the Los Alamos Sferic Array (LASA) as ground truth, *J. Atmos. Oceanic Technol.*, *23*(8), 1082–1092, doi:10.1175/JTECH1902.1.

Jacobson, A. R., R. Holzworth, and X.-M. Shao (2008), Low-frequency ionospheric sounding with narrow bipolar event lightning radio emissions: Energy-reflectivity spectrum, *Ann. Geophys.*, *26*(7), 1793–1803, doi:10.5194/angeo-26-1793-2008.

Jacobson, A. R., R. H. Holzworth, R. F. Pfaff, and M. P. McCarthy (2011a), Study of oblique whistlers in the low-latitude ionosphere, jointly with the C/NOFS satellite and the World-Wide Lightning Location Network, *Ann. Geophys.*, *29*(5), 851–863, doi:10.5194/angeo-29-851-2011.

Jacobson, A. R., R. H. Holzworth, M. P. McCarthy, and R. F. Pfaff (2011b), Initial studies with the lightning detector on the C/NOFS satellite, and cross validation with WWLLN, *J. Atmos. Oceanic Technol.*, *28*(11), 1423–1435, doi:10.1175/JTECH-D-11-00047.1.

Kelley, M. C., J. G. Ding, and R. H. Holzworth (1990), Intense ionospheric electric and magnetic field pulses generated by lightning, *Geophys. Res. Lett.*, *17*(12), 2221–2224.

Kelley, M. C., S. D. Baker, R. H. Holzworth, P. Argo, and S. A. Cummer (1997), LF and MF observations of the lightning electromagnetic pulse at ionospheric altitudes, *Geophys. Res. Lett.*, *24*(9), 1111–1114.

Klenzing, J., F. Simoes, S. Ivanov, R. A. Heelis, D. Bilitza, R. Pfaff, and D. Rowland (2011), Topside equatorial ionospheric density and composition during and after extreme solar minimum, *J. Geophys. Res.*, *116*, A12330, doi:10.1029/2011JA017213.

Lay, E. H., A. R. Jacobson, R. H. Holzworth, C. J. Rodger, and R. L. Dowden (2007), Local time variation in land/ocean lightning flash density as measured by the World Wide Lightning Location Network, *J. Geophys. Res.*, *112*, D13111, doi:10.1029/2006JD007944.

Maeda, K.-i., and I. Kimura (1959), Calculation of the propagation path of whistling atmospherics, *J. Atmos. Terr. Phys.*, *15*(1-2), 58–65.

Rybackek, S. T. (1995), Radio-wave propagation from antennae at satellite altitudes into the Earth-ionosphere wave-guide, *J. Atmos. Terr. Phys.*, *57*(3), 303–309, doi:10.1016/0021-9169(94)E0002-5.

Santolik, O., M. Parrot, U. S. Inan, D. Buresova, D. A. Gurnett, and J. Chum (2009), Propagation of unducted whistlers from their source lightning: A case study, *J. Geophys. Res.*, *114*, A03212, doi:10.1029/2008JA013776.

- Shaw, R. R., and D. A. Gurnett (1971), Whistlers with harmonic bands caused by multiple stroke lightning, *J. Geophys. Res.*, *76*(7), 1851–1854, doi:10.1029/JA076i007p01851.
- Sonwalkar, V. S., and U. S. Inan (1989), Lightning as an embryonic source of VLF hiss, *J. Geophys. Res.*, *94*(A6), 6986–6994, doi:10.1029/JA094iA06p06986.
- Thrane, E., and W. Piggott (1966), The collision frequency in the E- and D-regions of the ionosphere, *J. Atmos. Terr. Phys.*, *28*(8), 721–737, doi:10.1016/0021-9169(66)90021-3.
- Wait, J. R., and K. Spies (1960), Influence of Earth curvature and the terrestrial magnetic field on VLF propagation, *J. Geophys. Res.*, *65*(8), 2325–2331, doi:10.1029/JZ065i008p02325.